Exotic bonding interactions and coexistence of chemically distinct periodic lattice distortions in the charge density wave compound TaTe₂

Valeri Petkov [1,*], Kamal Chapagain [1], Junjie Yang,[2] Sarvjit Shastri,[3] and Yang Ren[3]

[1]*Department of Physics, Central Michigan University, Mt. Pleasant, Michigan 48858, USA*
[2]*Department of Physics, New Jersey Institute of Technology, Newark, New Jersey 07102, USA*
[3]*X-ray Science Division, Advanced Photon Source, Argonne National Laboratory, Argonne, Illinois 60439, USA*

The superstructure of TaTe₂ is examined by total high-energy x-ray scattering and large-scale structure modeling over a broad temperature range. At room temperature, it features double zigzag chains of Ta atoms exhibiting metallic bonding. The chains are sandwiched between planes of weakly interacting Te atoms. Below 170 K, the chains appear broken to "butterflylike" clusters and single zigzag chains of covalently bonded Te atoms emerge while Ta-Te interactions remain largely ionic. This is a rare example of a charge density wave compound stabilized by bonding that is a mix of covalent, ionic, and metallic character giving rise to chemically distinct periodic lattice distortions. We argue that the formation of periodic lattice distortions in the Te sublattice in addition to those in the Ta sublattice favors charge delocalization, which may explain the unusually diminished resistivity and increased magnetic susceptibility exhibited by the low-temperature charge density wave phase of TaTe₂. The effect may be common for $5d$ transition metal chalcogenides containing Te because of the extended electronic orbitals of the constituent atoms.

I. INTRODUCTION

Transition metal dichalcogenides (TMDs) exhibit a rich diagram of phases and fascinating properties resulting from interactions between electronic and crystal lattice degrees of freedom. Not surprisingly, these compounds provide a testbed to study complex physical phenomena in low-dimensional systems, including the interplay between charge density waves (CDWs) and superconductivity (SC) [1–6]. In particular, the octahedral polymorphs of Ta with Se ($1T$-TaSe₂) and Te ($1T'$-TaTe₂) have been found to exhibit CDW phases and no SC. However, mixed $1T$-TaSe₂₋ₓTeₓ compounds have been found to exhibit SC properties over a broad range of compositions in the middle of the phase diagram. Based on the observed falloff of the respective periodic lattice distortions (PLDs), the emergence of SC at low temperature has been related to the suppression of the CDW phase upon substituting Se and Te for one another [7–12]. Good atomic-level knowledge of the CDW phases of the end members of the series of $1T$-TaSe₂₋ₓTeₓ compounds is needed to understand the observed phenomena. However, contrary to the case of $1T$-TaSe₂, the CDW phases of $1T'$-TaTe₂ remain obscure [13–15]. This is because the phases have been studied by imaging and crystallographic techniques that are able to capture well the average crystal symmetry but may be less successful in revealing fine distortions of the underlying crystal lattice [16–20].

Here we use experimental techniques that are applicable to systems with any type of lattice distortions to study the superstructure of $1T'$-TaTe₂ over a broad temperature range,

including the transition between its room- (RT) and low-temperature (LT) phases. We confirm that the former involves double zigzag chains of Ta atoms exhibiting signatures of metallic bonding and a network of weakly interacting Te atoms. In the latter, the chains of Ta atoms appear broken to strings of disconnected "butterflylike" clusters. Furthermore, good portions of Te atoms organize in single zigzag chains exhibiting covalent bonding. The rest of Te atoms have their near nonbonding interactions largely unchanged. The partitioning of Te sublattice into extended segments of weakly and strongly interacting atoms and the related redistribution of charge may well explain the observed unusual decrease in the resistivity and increase in the magnetic susceptibility of the LT CDW phase of $1T'$-TaTe₂ in comparison to the RT CDW phase. The results expand our knowledge of the nature of CDW phases of TMDs and also demonstrate an experimental approach to study them in fine structural detail.

At an atomic level, $1T'$-TaTe₂ may be looked at as a stack of Ta-Te layers held together by weak van der Waals interactions. In a layer, an atomic plane of Ta atoms is sandwiched between two hexagonal planes of Te atoms, forming strong ionic bonds within a local octahedral unit [Fig. 1(e)]. In contrast to $1T$-TaSe₂, the octahedra in $1T'$-TaTe₂ are distorted and Ta-Te layers appear buckled [9,18]. It is considered that the distortion is due to the lower electronegativity of Te in comparison to Se, leading to a relative weakening of Ta-Te bonds and a partial charge transfer from Te to Ta [1,2,12,21]. At room temperature, the structure is stabilized by Ta-Ta interactions of metallic character, leading to local clustering of Ta atoms into double zigzag chains and an overall monoclinic distortion of the crystal lattice. Alternatively, the monoclinic structure of RT $1T'$-TaTe₂ can be regarded as distorted by a CDW that can be described in terms of a 3×1

*Corresponding author: petko1vg@cmich.edu
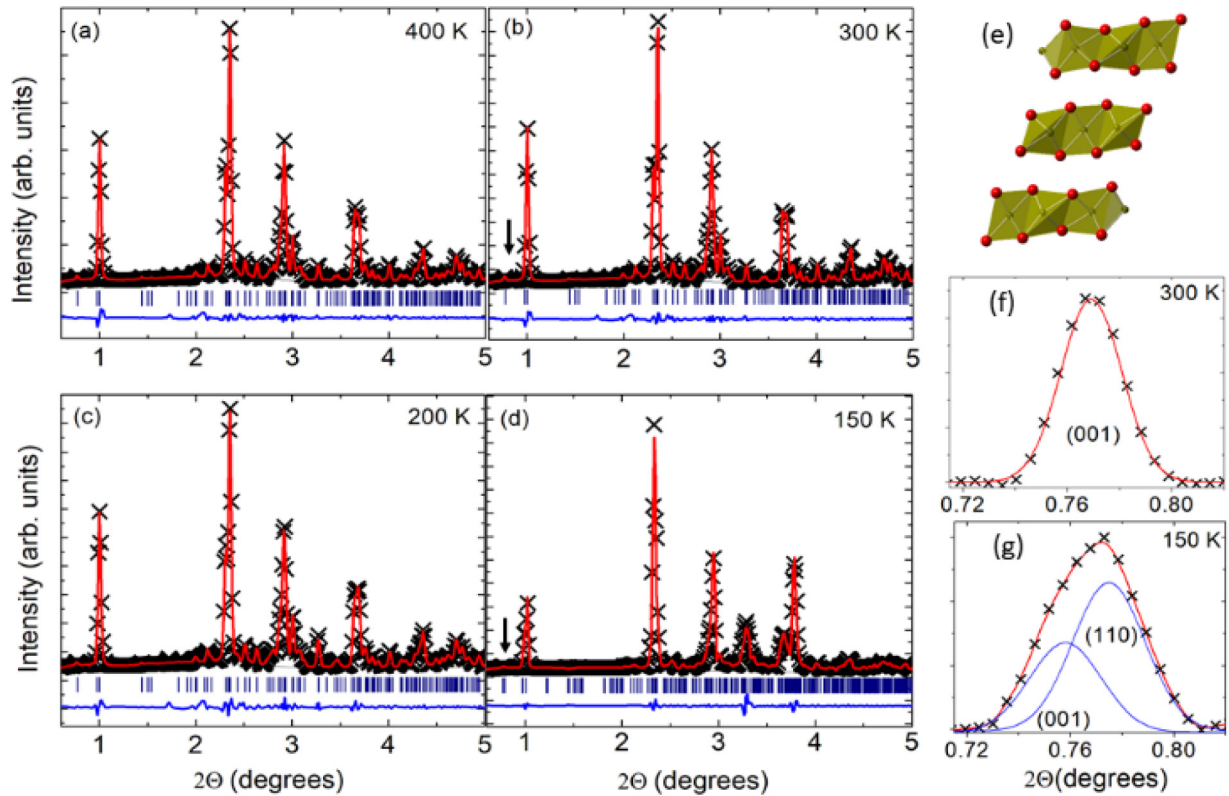
FIG. 1. (a)–(d) Rietveld fit (red line) to high-energy XRD patterns (symbols) for $1T'$-TaTe$_2$ collected at different temperatures. The residual difference (blue line) is shifted by a constant factor for clarity. All fits are satisfactory. (e) Fragment from the octahedral (brown) Ta-Te layers in $1T'$-TaTe$_2$. Ta atoms are in brown and Te atoms are in red. Fits (red line) to corresponding peaks (symbols) in the XRD patterns for $1T'$-TaTe$_2$ obtained at 300 and 150 K, i.e., at temperature above and below the transition temperature of 170 K, are shown in (f) and (g), respectively. The peaks are marked with vertical black arrows in the respective XRD patterns. The single (001) Bragg peak observed at 300 K is seen to turn into a doublet at 150 K, reflecting the tripling of the monoclinic unit cell. Using that cell, the components (blue line) of the doublet can be indexed as (001) and (110) Bragg peaks. The refined lattice parameters are shown in Fig. S1 of the Supplemental Material [28]. Note that (001) and (110) Bragg peaks shown in (g) are not well-resolved because the data are obtained using x rays with very high energy, leading to a significant "compression" of the XRD patterns toward low diffraction angles. High-energy x rays are needed for atomic PDF analysis [19,20].

superstructure based on a hypothetical undistorted $1T$-TaTe$_2$ lattice. Monoclinic $1T'$-TaTe$_2$ undergoes a structural phase transition at about 170 K, where the double zigzag chains of Ta atoms have been suggested to break down to strings of disconnected butterflylike clusters. The resulting PLDs have been described in terms of a 3×3 superstructure with an overall monoclinic symmetry. The transition is accompanied by a puzzling decrease in the resistivity and increase in the magnetic susceptibility [22,23], posing a question of whether the 3×3 superstructure is related to a CDW. That is because, usually, the emergence of a CDW results in reduced density of states at the Fermi level, leading to an increase in the resistivity and decrease in the magnetic susceptibility as observed with $1T$-TaSe$_2$ [24–27] . To add to the confusion, both the assembling of Ta atoms in RT $1T'$-TaTe$_2$ in double zigzag chains and the disintegration of these chains into butterflylike clusters in LT $1T'$-TaTe$_2$ have been challenged recently [13]. To resolve the controversy, we studied $1T'$-TaTe$_2$ by conventional and resonant high-energy x-ray diffraction (XRD) coupled to atomic pair distribution function (PDF) analysis and reverse Monte Carlo (RMC) simulations. The studies were conducted over a wide temperature range from 400 to 100 K, including the RT to LT CDW phase transition. Fine

details of the local atomic arrangement of Ta and Te atoms were revealed and examined to highlight the distinct PLDs in RT and LT $1T'$-TaTe$_2$.

II. EXPERIMENT

The polycrystalline $1T'$-TaTe$_2$ sample was made by conventional solid-state synthesis described in the Supplemental Material (SM) [28]. It was subjected to XRD experiments using synchrotron x rays with energy of 105.7 keV ($\lambda = 0.1173$ Å). Note that using high-energy x rays is necessary to achieve high wave vectors and hence obtain PDFs with high-real-space resolution. As shown below, this allows us to probe fine differences between the PLDs in RT and LT $1T'$-TaTe$_2$. Details of synchrotron XRD experiments are given in the SM. Exemplary XRD patterns collected at different temperature and results from Rietveld fits to the patterns are shown in Figs. 1(a)–1(d). The fits confirm the monoclinic symmetry (*S.G.* $C2/m$) of the average crystal structure of both RT and LT $1T'$-TaTe$_2$. As can be seen in Fig. S1 of the SM [28], the a and c parameters of the monoclinic unit cell of $1T'$-TaTe$_2$ diminish gradually with decreasing temperature. However, the b parameter sharply increases by a factor of 3 below 200 K,
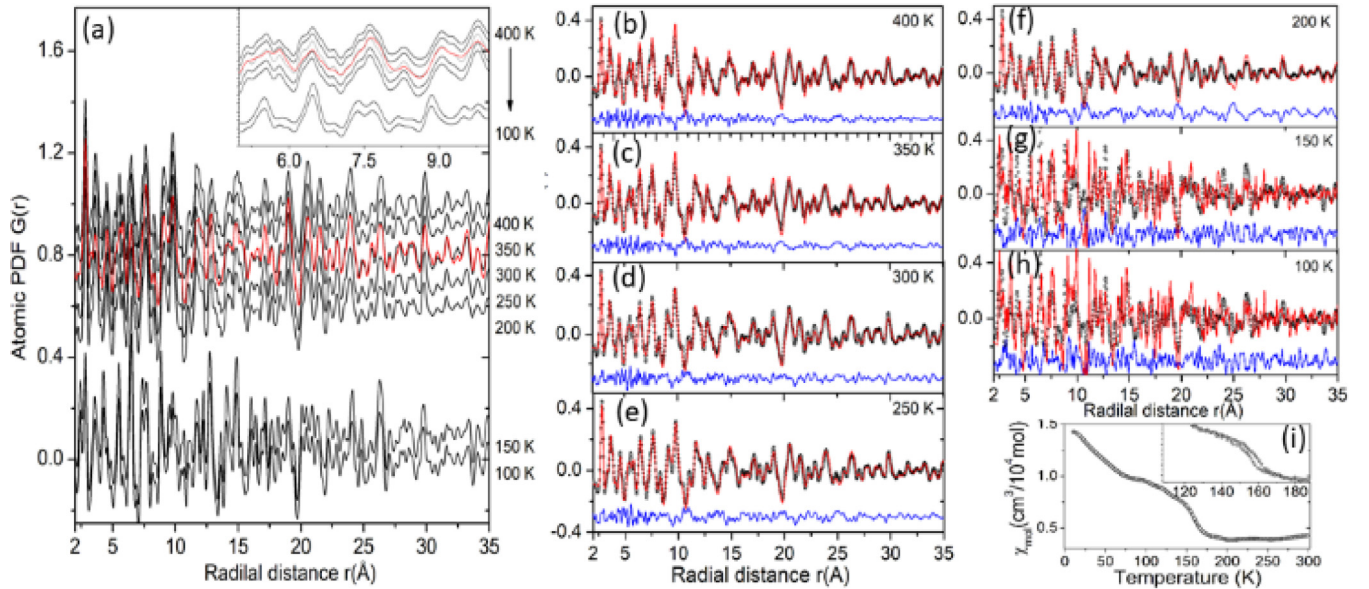
FIG. 2. (a) Experimental total (black line) and Ta-differential (red line) atomic PDFs for $1T'$-$TaTe_2$ obtained at different temperatures. A segment of the low-r region of the PDFs is shown in the inset. PDF peak position and particularly relative intensity change significantly below 200 K. (b)–(h) Traditional crystallography constrained fits (red line) to the experimental (symbols) total PDFs. The residual difference (blue line) is shifted by a constant factor for clarity. Fits to the data obtained at 200 K and above are based on a previously suggested 3×1 double zigzag chain superstructure [Fig. 3(a)] that can be described in terms of an 18-atom monoclinic unit cell. The fits are satisfactory. Fits to the data sets obtained at 150 and 100 K are based on a previously suggested 3×3 string of butterflylike clusters superstructure [Fig. 4(a)] that can be described in terms of a 54-atom monoclinic unit cell. The fits are unsatisfactory, indicating that the model does not capture well all details of the local atomic structure of LT $1T'$-$TaTe_2$. (i) Molar magnetic susceptibility for $1T'$-$TaTe_2$ as a function of temperature. Data are corrected for the diamagnetic core electrons contribution. The susceptibility exhibits a sharp increase at temperature of approximately 170 K. A clear hysteresis is observed indicating that the transition is first order.

reflecting the tripling of the unit cell at low temperature. Exemplary Bragg peaks sensitive to the tripling are shown in Figs. 1(f) and 1(g). Experimental atomic PDFs derived from the XRD patterns are shown in Fig. 2(a). As defined, atomic PDFs peak at distances separating frequently occurring pairs of atoms, and the areas under the peaks are proportional to the relative number of those pairs [19,20]. This renders atomic PDFs very sensitive to local lattice distortions in CDW compounds, including $1T'$-$TaTe_2$.

III. EXPERIMENTAL DATA ANALYSIS AND 3D STRUCTURE MODELING

As can be seen in Fig. 2(a), the position and particularly the relative intensity of PDF peaks change significantly below 200 K. The observation indicates that, though both monoclinic on average, the RT and LT CDW phases of $1T'$-$TaTe_2$ exhibit significantly different PLDs. In line with the findings of prior studies [9], the magnetic susceptibility shows a sharp increase at about 170 K [Fig. 2(i)], illustrating the strong correlation between the lattice and electronic degrees of freedom in $1T'$-$TaTe_2$.

To verify the previously suggested 3×1 double zigzag chain superstructure of RT $1T'$-$TaTe_2$ [Fig. 3(a)], the experimental PDFs obtained at temperature 200 K and above were approached with a model based on its well-known 18-atom monoclinic unit cell [9]. In the cell, Ta atoms occupy two different Wyckoff positions. The so-called Ta1 atoms occupy the centers of less distorted Ta-Te_6 octahedra aligned along

the cell's b direction. They form the interior of the double zigzag chains of Ta atoms. The rim of the chains is formed by the so-called Ta2 atoms [Fig. 3(a)] centering more distorted Ta-Te_6 octahedra. Thus, the Ta1-Te2 and Ta2-Ta2 distances of closest approach appear equal to 3.3 and 4.4 Å, respectively [Fig. 3(b)].

As can be seen in Figs. 2(b)–2(f), the double zigzag chain model based on the 18-atom crystallographic unit cell approaches the experimental PDF data obtained at 200 K and above closely, which corroborates the validity of the model. Nevertheless, we conducted a complementary resonant high-energy XRD experiment at the K edge of Ta. The resulting Ta-differential atomic PDF reflects only structural features involving Ta atoms, providing extra sensitivity to the type of their arrangement in the RT CDW phase of $1T'$-$TaTe_2$ [29]. Experimental details are given in the SM [28]. We also constructed a large-scale structure model and refined it against the respective total and Ta-differential PDF data using reverse Monte Carlo (RMC) simulations. The model featured a 120 Å $\times$ 120 Å $\times$ 100 Å configuration of 74 851 Ta and Te atoms cut out from the monoclinic lattice of RT $1T'$-$TaTe_2$. Its large size allowed us to explore Ta-Ta pair correlations extending well beyond the crystallographic 18-atom unit cell. Modeling details are given in the SM [28]. As can be seen in Figs. S1(c) and S1(d) of the SM [28], the RMC refined model fits the experimental PDF data very well. Fragments of the model are shown in Figs. 3(b)–3(d). They clearly show the presence of double zigzag chains of Ta atoms. Notably, the RMC refined model also reproduced the atomic PDF data
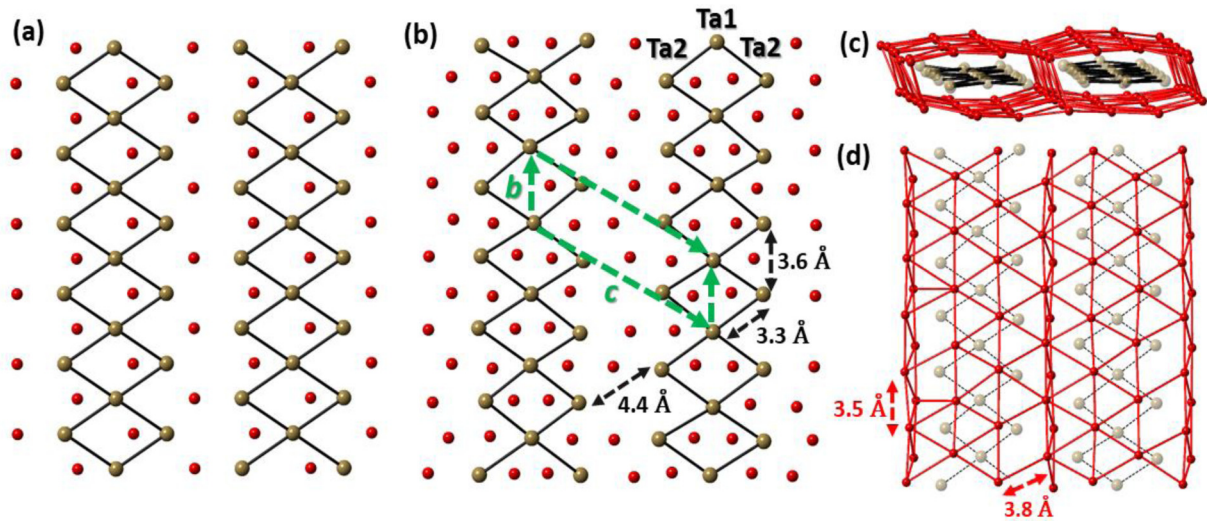
FIG. 3. Top view of a single Ta plane in the (a) ideal and (b) RMC refined 3×1 double zigzag chain (black line) superstructure of RT $1T'$-TaTe$_2$. The b and c axes of the monoclinic unit cell are given as dotted green lines. Also shown in (b) are characteristic Ta-Ta distances. Atoms labeled as Ta1 and Ta2 occupy, respectively, Wyckoff position $2a$ and $4i$ in the cell. (c) Side view of a single Ta-Te layer in RT $1T'$-TaTe$_2$ comprising a single Ta plane sandwiched between two planes of Te atoms. The latter appear slightly buckled in the area between the double zigzag chains of Ta atoms. This is likely because the specific clustering of Ta atoms would reduce the overlap between Te $5p$ and Ta $5d$ valence orbitals in that area. To recover the overlap, nearby Te atoms move toward Ta planes. Note that the observed buckling is much less expressed than that exhibited by LT $1T'$-TaTe$_2$ [compare with data in Fig. 4(c)]. (d) Top view of the network of Te atoms in one Ta-Te layer with exemplary Te-Te distances (red arrows) shown. Altogether, Te-Te distances in Te planes range from 3.35 to 3.9 Å. Data in (b)–(d) are computed from atomic positions obtained by mapping the respective RMC model onto a single Ta-Te layer. Ta atoms are in light brown and Te atoms are in red.

sets obtained well above (350 and 400 K) and below (250 and 200 K) room temperature [see Figs. S1(a) and S1(b) and Figs. S1(e) and S1(f), respectively [28]]. Thus, both 18-atom crystallographic unit cell constrained modeling and large-scale RMC simulations based on 74 851-atom configurations converged to the same 3×1 double zigzag chain superstructure of RT $1T'$-TaTe$_2$, providing strong evidence in support of its validity. Evidently, the ionic-type Ta-Te bonding and double zigzag chains of Ta atoms exhibiting metallic-type bonding render the RT CDW phase of $1T'$-TaTe$_2$ stable over a broad temperature region, extending from 400 K down to 170 K. As shown below, the situation with the LT CDW phase of $1T'$-TaTe$_2$ is different. Here it may be added that the recently suggested Ta-Ta dimer model for RT $1T'$-TaTe$_2$ [13] features Ta2-Ta2 distances that are significantly shorter than Ta1-Ta2 distances. The presence of such short Ta2-Ta2 is not supported by the results of PDF analysis and structure modeling done here.

To verify the previously suggested 3×3 strings of butterflylike clusters superstructure of LT $1T'$-TaTe$_2$ [Fig. 4(a)], the experimental PDFs obtained at temperatures 150 and 100 K were approached with a model based on its well-known 54-atom monoclinic unit cell [9]. As can be seen in Figs. 2(g) and 2(h), the model, which otherwise is largely consistent with the experimental XRD data [Fig. 1(d)], does not reproduce the experimental PDF data well. The misfit indicates a significant divergence of the local atomic structure of LT $1T'$-TaTe$_2$ from the average crystal structure. To resolve the problem, the experimental PDFs obtained at 100 and 150 K were approached with a large-scale structure model using RMC simulations. The initial model featured a 120 Å $\times$ 110 Å $\times$

100 Å configuration of 70 524 Ta and Te atoms obtained by stacking together replicas of the 54-atom monoclinic unit cell of LT $1T'$-TaTe$_2$. As can be seen in Figs. S1(g) and S1(h) [28], the RMC refined model reproduces the experimental PDFs in very good detail. A stack of four Ta-Te layers in the refined model is shown in Fig. 5. A more detailed fragment of the model is shown in Figs. 4(c)–4(e). Analysis of the model indicates that, contrary to the findings reported in Ref. [13] and in line with the findings of prior single-crystal XRD [9], Ta atoms in LT $1T'$-TaTe$_2$ assemble into butterflylike clusters forming a characteristic 3×3 superstructure [Fig. 4(b)]. This superstructure is closely related to the 3×1 superstructure of Ta atoms in RT $1T'$-TaTe$_2$ [Fig. 4(b)]. The difference between the two superstructures is that Ta1-Ta1 distances in RT $1T'$-TaTe$_2$ are uniform and equal to 3.6 Å [see the interior of the double zigzag chains in Fig. 3(b)] whereas Ta1-T1 distances in LT $1T'$-TaTe$_2$ show a modulation with two short distances of 3.3 Å alternating with a long one of 4.2 Å [see the strings of butterflylike clusters in Fig. 4(b)]. However, the positions of Te atoms in the RMC refined model and the single-crystal XRD derived models for LT $1T'$-TaTe$_2$ appear significantly different.

In particular, Te atoms positioned immediately above and below the "empty" space between the strings of butterflylike Ta clusters appear considerably closer together in comparison to the findings of single-crystal XRD. Notably, the emerged Te-Te distances of 2.9 Å also appear considerably shorter than the corresponding distances of 3.5 Å in RT $1T'$-TaTe$_2$ [compare Te-Te distances in Fig. 3(d), 4(d), and 4(e)]. Likely, this is because the disintegration of double zigzag chains in RT $1T'$-TaTe$_2$ into strings of butterflylike clusters in LT
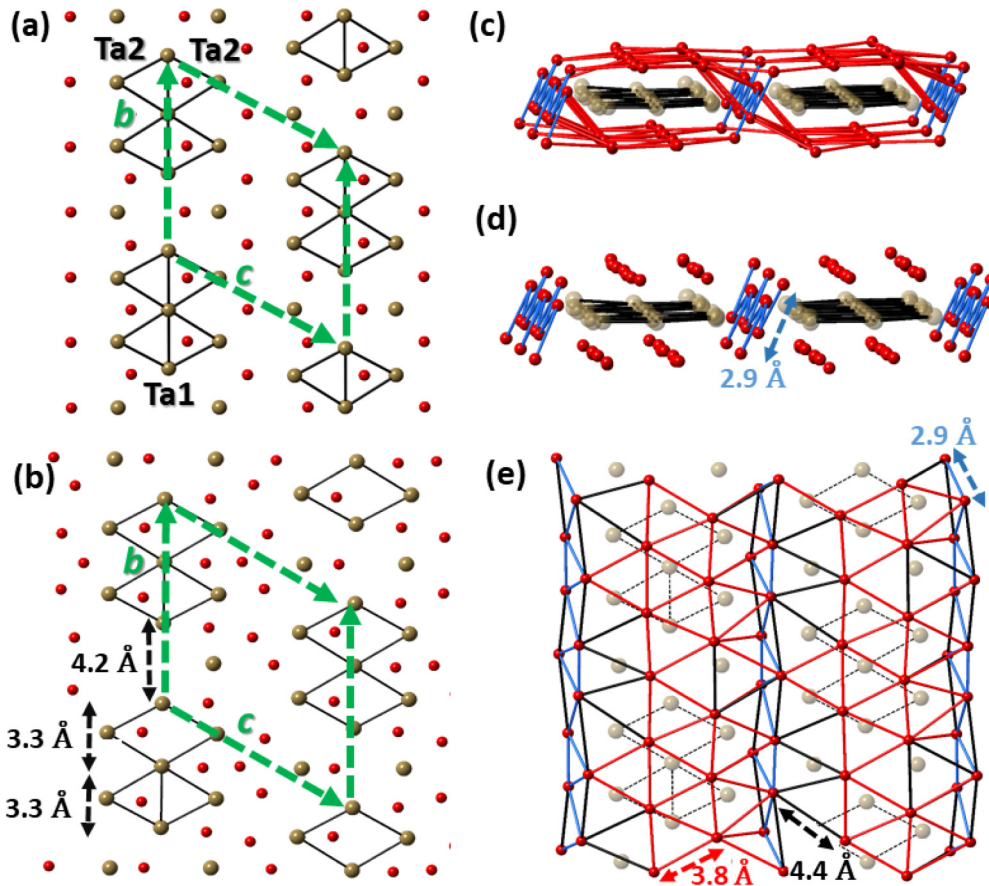
FIG. 4. Top view of a single Ta plane in the (a) suggested and (b) RMC refined 3×3 superstructure of LT $1T'$-TaTe$_2$ at 100 K. The b and c axes of the unit cell are given as doted green lines. Also shown in (a) and (b) are characteristic distances (black line) between nearby Ta atoms. The atoms exhibit metallic-type interactions resulting in the formation of strings of disconnected butterflylike clusters. Atoms labeled as Ta1 and Ta2 are those defined in Fig. 3(b). (c) Side view of a single Ta-Te layer comprising a single Ta plane sandwiched between two Te planes. For reasons discussed in the text, the "buckling" of Te planes in the area between the chains of Ta clusters is much larger than that in RT $1T'$-TaTe$_2$ [compare with data in Fig. 3(c)]. It results in Te-Te distances shorter than 3 Å (blue line), indicating covalent bonding. (d) Side view of a single Ta-Te layer emphasizing the zigzag chains of Te atoms running in parallel to the strings of butterflylike clusters of Ta atoms. (e) Top view of the network of Te atoms in LT $1T'$-TaTe$_2$. The network exhibits Te-Te distances shorter than 3 Å (blue line) characteristic to strong covalent-type interactions, in the range from 3.1 to 3.9 Å (red line) characteristic to multicenter bonding interactions, and from 3.9 to 4.5 Å (black line) characteristic to nonbonding, van der Walls-type interactions. Data in (b–e) are computed from atomic positions obtained by mapping the respective RMC model onto a single Ta-Te layer. Ta atoms are in light brown and Te atoms are in red.

$1T'$-TaTe$_2$ upon cooling reduces further the overlap between the Te $5p$ and Ta $5d$ valence orbitals in that space. To recover the overlap and stabilize the specific LT $1T'$-TaTe$_2$ structure, Te atoms in its vicinity move even closer to Ta planes between them. As a result, single zigzag chains of covalently bonded Te atoms emerge [Figs. 4(d) and 4(e)]. The chains run in parallel to the strings of butterflylike Ta clusters, indicating that these two different types of PLDs are likely to be strongly correlated. Remarkably, Te-Te distances of 2.90 Å in the chains fall well below the sum of the van der Waals radii (4.2 Å) for Te atoms. Indeed, they appear close to the single covalent Te-Te bond length (2.83 Å) in elemental Te, indicating an increased interaction between Te atoms in the chains in comparison to Te atoms not participating in the chains. Here it is worthwhile to mention that the relatively short Te-Ta contacts resulting from the shift of Te atoms toward Ta planes may be viewed at as a result of a particular local atomic packing required by

the LT $1T'$-TaTe$_2$ structure to accommodate the alternating strings of metallic-type Ta clusters and single zigzag chains of covalently bonded Te atoms, and not as an actual Ta-Te bond.

IV. DISCUSSION

The picture which emerges is as follows: Based on conventional bonding theory, each Ta and Te atom in $1T'$-TaTe$_2$ would be assigned a formal charge of $+4$ and -2, respectively, and the Ta-Te bond would be considered as ionic in character. In metals, however, the electrons cannot be as localized as implied by an oxidation state formalism. This is particularly true for $1T'$-TaTe$_2$, where the relatively low electronegativity of Te results in a charge transfer from Te to Ta. As a result, Ta-Ta bonding acquires some metal character and Ta atoms cluster into double zigzag chains already well above room temperature. The diminished charge of Te atoms
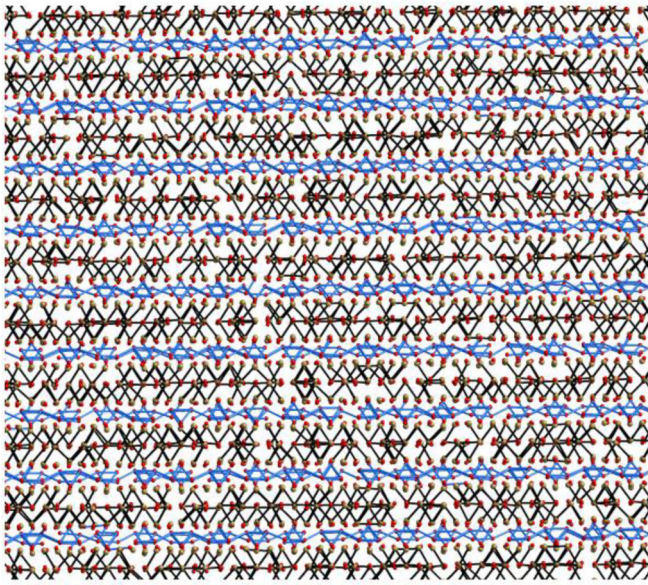
FIG. 5. Top view of a stack of four Ta-Te layers in the RMC refined model for LT $1T'$-TaTe$_2$, where each layer is made of a plane of Ta atoms (brown) sandwiched between planes of Te atoms (red). Black lines represent Ta-Ta distances shorter than 3.3 Å and blue lines represent Te-Te distances shorter than 3.1 Å. As can be seen in the figure, Ta atoms form parallel strings of butterflylike clusters and Te atoms form zigzag chains positioned in between the strings. This is a rare example of a CDW compound exhibiting two chemically distinct periodic lattice distortions. Notably, prior imaging experiments also indicated the presence of more than one distinct charge modulations in LT $1T'$-TaTe$_2$ [13]. Note that, due to surface reconstruction effects, otherwise distinct modulations can appear somewhat entangled for surface sensitive techniques. By contrast, the XRD-based results presented here appear as a quantity averaged over the sample volume probed by the x-ray beam, which is approximately 0.5 mm × 0.5 mm × 1.0 mm in our case.

induces attractive Te-Te bonding interactions manifested by the observed shortening of some Te-Te distances down to 3.5 Å [Fig. 3(d)], which is well below the sum of respective van der Waal radii.

In LT $1T'$-TaTe$_2$, Ta-Ta interactions and Ta clustering are modified. In turn, single zigzag chains of strongly interacting Te atoms appear, exhibiting further shortened Te-Te distances of 2.9 Å. At the same time, distances between Te atoms in the chains and nearby Te atoms not involved in the chains appear elongated to 4.4 Å, which is well beyond their value of 3.8 Å in RT $1T'$-TaTe$_2$ [compare data in Figs. 3(d) and 4(e)]. This indicates a weakening of the bonding interactions between the former and the latter. Generally, the partitioning of a network of Te atoms into alternating segments exhibiting near nonbonding and strong covalent bonding interactions, in particular parallel zigzag chains [blue lines in Figs. 4(d), 4(e), and 5], favor charge delocalization along the network [30–32]. Such charge delocalization and the likely increase in DOS at the Fermi level may well explain the decrease in the resistivity and increase in the magnetic susceptibility of $1T'$-TaTe$_2$

taking place when its LT CDW phase emerges upon cooling. Regardless of the unusual change in the transport and magnetic properties, the transition between RT and LT $1T'$-TaTe$_2$ may still be considered to be of CDW type simply because it involves the formation of PLDs in the Te sublattice, which are not well-expressed above the transition temperature.

V. CONCLUSION

Our structure studies confirm the 3×1 double zigzag chain superstructure of Ta atoms in RT $1T'$-TaTe$_2$. They also confirm the 3×3 strings of disconnected butterflylike clusters superstructure of Ta atoms in LT $1T'$-TaTe$_2$. In the latter, a PLD featuring single zigzag chains of covalently bonded Te atoms is also revealed, indicating the presence of both unusually diverse interactions between the constituent atoms and strong electron-lattice coupling in $1T'$-TaTe$_2$. These lead to a complex landscape of PLDs, as follows: At high temperature, the CDW phase of $1T'$-TaTe$_2$ is stabilized by Ta-Te interactions of ionic and Ta-Ta interactions of metallic character, where the latter are manifested by clustering of Ta atoms into double zigzag chains. Weak bonding interactions between Te atoms are also likely to exist because some Te-Te distances appear shorter than the sum of van der Waals radii. At low temperature, the competition for valence electrons between the constituent atoms results in further charge redistribution. It leads to breaking of Ta double zigzag chains to strings of butterflylike clusters and concurrent formation of single zigzag Te chains running alongside these strings. Altogether, the structural transition between the high- and low-temperature CDW phases of $1T'$-TaTe$_2$ appears to be driven by charge redistribution effects involving significant changes in the type and strength of Ta-Ta and Te-Te interactions. A similar mechanism, including the formation of Ir-Ir and Te-Te dimers, has been suggested as a driving force behind the phase transition between the RT and LT CDW phases of IrTe$_2$ [33]. In $1T'$-TaTe$_2$, however, metal-metal and chalcogenide-chalcogenide interactions appear stronger in comparison to IrTe$_2$ leading to coexisting periodic distortions in the Ta and Te sublattices at low temperature. This renders LT $1T'$-TaTe$_2$ a rare example of a CDW compound where two chemically distinct PLDs coexist and, furthermore, the delocalization of electron density increases in comparison with the RT CDW phase. In general, such effects may be expected to occur in $5d$ transition metal tellurides because of the extended electronic orbitals of the constituent atoms and, therefore, may need to be accounted for in studies on the interplay between CDWs and superconductivity exhibited by these systems.

[1] K. Rossnagel, J. Phys.: Condens. Matter. **23**, 213001 (2011).

[2] X. Zhu, J. Guo, J. Zhang, and E. W. Plummer, Adv. Phys.: X **2**, 622 (2017).

[3] C.-W. Chen, J. Choe, and E. Morrosan, Rep. Prog. Phys. **79**, 084505 (2016).

[4] U. Chatterjee, J. Zhao, M. Iavarone, R. Di Capua, J. P. Castella, G. Karappetkov, C. D. Mallakas, M. G. Kanatzidis, H. Claus, J. P. C. Ruff, F. Weber, J. van Wezel, J.C. Campuzano, R. Oswborn, M. Randeria, N. Trivedi, M. R. Norman, and S. Rozenkranz, Nat. Commun. **6**, 6313 (2015).

[5] L. Li, X. Deng, Z. Wang, Y. liu, M. Abeykoon, E. Dooryhee, A. Tomic, Y. Huang, J. B. Warren, E. S. Bozin, S. J. L. Billinge, Y. Sun, Y. Zhu, G. Kotliar, and C. Petrovic, npj Quant. Mater. **2**, 11 (2017).

[6] H. Lou, W. Xie, J. Tao, H. Inoe, A. Gyenis, J. W. Kristan, A. Yazdani, Y. Zhu, and R. J. Cava, Proc. Natl. Acad. Sci. **112**, E1174 (2015).

[7] A. W. Tsen, R. Hovden, D. Wang, Y. D. Kim, J. Okamoto, K. A. Spoth, Y. Liu, W. Lu, Y. Sun, J. C. Hone, L. F. Kourkoutis, P. Kim, and A. N. Pasupathy, Proc. Natl. Acad. Sci. USA **112**, 15054 (2015).

[8] G. H. Han, D. L. Duong, D. H. Keum, S. J. Yun, and Y. H. Lee, Chem. Rev. **118**, 6297 (2018).

[9] T. Sorgel, J. Nuss, U. Wedig, R. K. Kremer, and M. Jansen, Mat. Res. Bull. **41**, 987 (2006).

[10] H. Yang, S. W. Kim, M. Chhowalla, and Y. H. Lee, Nat. Phys. **13**, 931 (2017).

[11] Y. Liu, D. F. Shao, L. J. Li, W. J. Lu, X. D. Zhu, P. Tong, R. C. Xiao, L. S. Ling, C. Y. Xi, L. Pi, H. F. Tian, H. X. Yang, J. Q. Li, W. H. Song, X. B. Zhu, and Y. P. Sun, Phys. Rev. B **94**, 045131 (2016).

[12] D. C. Miller, S. D. Mahanti, and P. M. Duxbury, Phys. Rev. B **97**, 045133 (2018).

[13] J. Feng, A. Tan, S. Wagner, J. Liu, Z. Mao, X. Ke, and P. Zhang, Appl. Phys. Lett **109**, 021901 (2016).

[14] J. J. Gao, J. G. Si, X. Luo, J. Yan, F. C. Chen, G. T. Lin, L. Hu, R. R. Zhang, P. Tong, W. H. Song, X. B. Zhu, W. J. Lu, and Y. P. Sun, Phys. Rev. B **98**, 224104 (2018).

[15] C. Chen, H.-S. Kim, A. S. Admasu, S.-W. Cheong, K. Haule, D. Vanderbilt, and W. Wu, Phys. Rev. B **98**, 195423 (2018).

[16] S. van Smaalen, Acta Crystallogr. Sect. A: Found. Adv. **A61**, 51 (2005).

[17] H. J. Kim, C. D. Malliakas, A. T. Tomic, S. H. Tessmer, M. G. Kanatzidis, and S. J. L. Billinge, Phys. Rev. Lett. **96**, 226401 (2006).

[18] A. Vernes, H. Ebert, W. Bensch, W. Heid, and C. Näther, J. Phys.: Condens. Matter **10**, 761 (1998).

[19] T. Egami and S. J. L. Billinge, *Underneath the Bragg Peaks: Structural Analysis of Complex Materials* (Pergamon, Oxford, England, 2003).

[20] V. Petkov, *Characterization of Materials* (John Wiley & Sons, New York, 2012), pp. 1361–1372.

[21] M.-L. Doublet, S. Remy, and F. Lemoigno, J. Chem. Phys. **113**, 5879 (2000).

[22] H. Chen, Z. Li, L. Guo, and X. Chen, Europhys. Lett. **117**, 27009 (2017).

[23] C. Ayache, R. Currat, B. Hennion, and P. Moline, J. de Physique IV Colloque **3**, C2-125 (1993).

[24] A. M. Gabovich, A. I. Voitenko, J. F. Annett, and M. Ausloos, Superconduct. Sci. Technol. **14**, R1 (2001).

[25] W. Choi, N. Choudhary, G. H. Han, J. Park, D. Akinwande, and Y. H. Lee, Mat. Today **20**, 116 (2017).

[26] L.-L. Wei, S.-S. Sun, K. Sun, Y. Liu, D.-F. Shao, W.- J. Lu, Y.-P. Sun, H.-F. Tian, and H.-X. Yang, Chin. Phys. Lett. **34**, 086101 (2017).

[27] H. W. Myron, J. Rath, and A. J. Freeman, Phys. Rev. B **15**, 885 (1977).

[28] See Supplemental Material at http://link.aps.org/supplemental/10.1103/PhysRevB.102.024111 for details about x-ray-diffraction experiments and structure modeling, which includes Refs. [9,13,34–37].

[29] V. Petkov, S. Shastri, J.-W. Kim, S. Shan, J. Luo, J. Wu, and Ch.-J. Zhong, Acta Crystallogr., Sect. A **74**, 553 (2018).

[30] R. Patschke and M. G. Kanatzidis, Phys. Chem. Chem. Phys. **4**, 3266 (2002).

[31] X. Zhang, J. Li, B. Foran, S. lee, H.-Y. Guo, T. Hogan, C. R. Cannewurf, and M. G. Kanatzidis, J. Am. Chem. Soc. **117**, 10513 (1995).

[32] C. Graf, A. Assoud, O. Maysree, and H. Kleinke, Molecules **14**, 3115 (2009).

[33] G. L. Pascut, K. Haule, M. J. Gutmann, S. A. Barnett,A. Bombardi, S. Artyukhin, T. Birol, D. Vanderbilt, J. J. Yang, S.-W. Cheong, and V. Kiryukhin, Phys. Rev. Lett. **112**, 086402 (2014).

[34] B. H. Toby and R. B. Von Dreele, J. Appl. Crystallogr. **46**, 544 (2013).

[35] C. L. Farrow, P. Juhas, J. Liu, D. Bryndin, E. S. Božin, J. Bloch, Th. Proffen, and S. J. L. Billinge, J. Phys: Condens. Matter **19**, 335219 (2007).

[36] V. Petkov and S. Shastri, Phys. Rev. B **81**, 165428 (2010).

[37] O. Gereben and V. Petkov, J. Phys.: Condens. Matter **25**, 454211 (2013).